

Kraft Mesh Origami for Efficient Oil–Water Separation

Yu-Qing Liu,[†] Zhi-Zhen Jiao,[†] Yong-Lai Zhang,^{*,†} Yan Liu,[‡] Hao-Bo Jiang,[‡] Dong-Dong Han,[†] and Hong-Bo Sun[§]

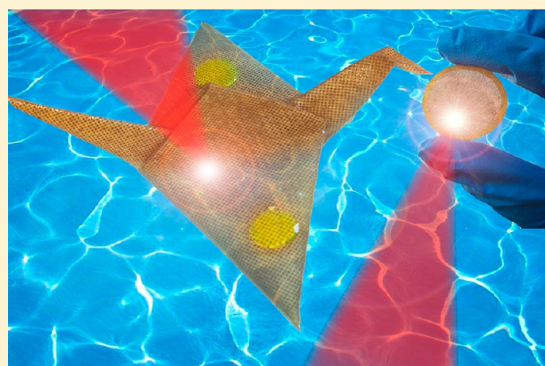
[†]State Key Laboratory of Integrated Optoelectronics, College of Electronic Science and Engineering, Jilin University, Changchun 130012, China

[‡]Key Laboratory of Bionic Engineering (Ministry of Education), Jilin University, Changchun 130022, China

[§]State Key Lab of Precision Measurement and Instruments, Department of Precision Instrument, Tsinghua University, Beijing 100084, China

Supporting Information

ABSTRACT: Inspired from fish scales that exhibit unique underwater superoleophobicity, artificial porous membranes featuring similar wettability have been successfully developed for oil–water separation. However, most of the superoleophobic meshes are workable only for underwater oil/water separation and become disabled in air. In this article, we reported the facile fabrication of underwater superoleophobic kraft mesh and demonstrated efficient oil–water separation using kraft mesh origamis. Kraft paper that features porosity, natural hydrophilicity, and relatively high elasticity and tear resistance has been found to be an ideal candidate for developing underwater superoleophobic origami. Direct laser drilling has been employed to make microhole arrays on the kraft paper, forming a flexible mesh. The hydrophilic nature and the hierarchical microstructures that consist of microhole arrays and porous microfiber networks make the resultant kraft mesh superoleophobic underwater, enabling oil–water separation. More importantly, the kraft mesh can retain a large amount of water (2.5 times its weight under dry conditions) owing to its porous and hydrophilic structure. Thus, the wet kraft mesh became a slippery surface for oil droplets when it was taken out of the water. This unique feature makes it possible to directly fish out oil droplets from water using a simple kraft mesh origami. Direct laser drilling of paper mesh for flexible origami may open up a new route to the rational design and fabrication of oil–water separation devices.



INTRODUCTION

Natural creatures always possess promising properties due to the presence of almost perfect micronanostructures. Learning from natural nanostructures has been considered to be a shortcut to the design and development of artificial functional devices. Recently, there has been growing research interest in developing bioinspired nanostructures toward cutting-edge applications such as drug delivery and soft robotics.^{1–4} For instance, bioinspired functional surfaces that possess superwettability can always lead to unique properties or functionalities.^{5–12} In particular, functional membranes with precise design wettability are promising for a wide range of applications including water treatment, advanced separation, drug delivery, and tissue engineering.^{13–16} Toward antioil applications such as oil–water separation, two kinds of typical membranes, superhydrophobic^{17–20} and underwater superoleophobic membranes,^{21–23} have been intensively investigated. In the former case, oils can pass through the oleophilic membranes, whereas water cannot pass through them due to the superhydrophobicity. However, considering the fact that most oils are lighter than water, in most cases, water may get in touch with the membranes first due to their relatively large

density. Therefore, the latter kind of membrane may be more suitable for practical use. The development of underwater superoleophobic membranes for oil–water separation was inspired by fish scales that present superoleophobicity and low oil adhesion at an oil/water/solid three-phase interface.²⁴ The unique wettability of fish scales can be attributed to the presence of hydrophilic micro/nanostructures. On the basis of the thorough understanding of the inherent mechanism, underwater superoleophobic surfaces have been successfully developed by using various hydrophilic materials according to a basic principle that the in-air superhydrophilicity is crucial to underwater superoleophobicity.^{22,24–28}

As typical examples, Jiang et al. first demonstrated the underwater superoleophobic membrane by using a hydrophilic hydrogel to coat a metal mesh.²⁵ After that, various hydrophobic materials have been attached to porous frameworks such as metal meshes,²⁶ membranes,²⁷ sponges,²⁹ and foams¹⁸ to produce underwater superoleophobic membranes

Received: October 23, 2018

Revised: November 29, 2018

Published: December 18, 2018

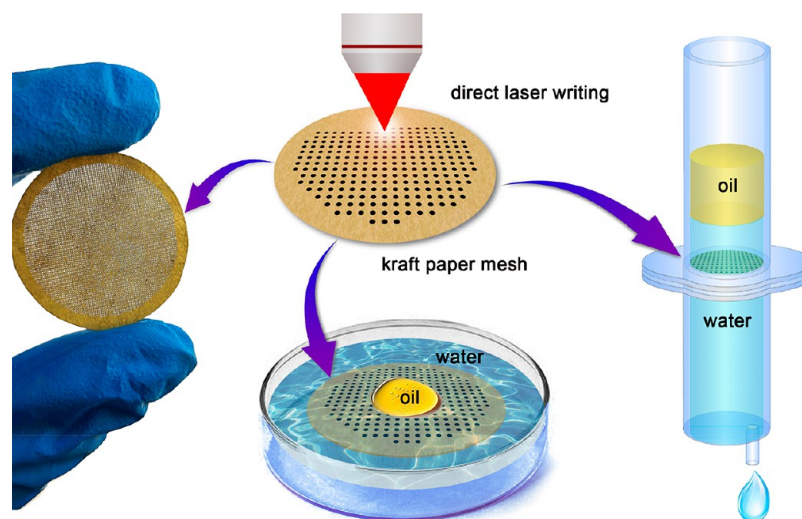


Figure 1. Schematic illustration of the laser fabrication of a paper-based oil–water separation membrane.

toward efficient oil–water separation applications. For instance, Jin et al. fabricated superhydrophilic and underwater superoleophobic poly(vinylidene difluoride) filtration membranes by grafting a layer of poly(acrylic acid) via a salt-induced phase-inversion approach.³⁰ Chen et al. reported the fabrication of underwater superoleophobic surfaces by combining a femtosecond laser and oxygen plasma treatments of PDMS.^{23,31} Yong et al. has achieved great success in efficient oil–water separation using natural porous materials directly.^{32–34} In our previous work,²¹ we used a thin layer of GO to coat a metal wire mesh to make a superhydrophilic and underwater superoleophobic surface, realizing efficient oil–water separation.

In spite of the above-mentioned advancements, functional meshes enabling oil–water separation are still far from practical applications due to the following limitations. First, the reported methods for producing underwater superoleophobic mesh usually involve complex fabrication procedures or depend on special materials, which limits their scaling-up production and practical applications. Besides, the dimensions of underwater superoleophobic meshes, generally prepared by material deposition,³⁵ layer-by-layer assembly,^{36,37} and “bottom-up” growth on porous frameworks,²⁶ are limited to a relatively small area. More importantly, most of the superoleophobic meshes or membranes are workable only when they are immersed in water. They may become disabled in air due to the loss of water. In that case, the oil/water/solid three-phase interface may become the oil/air/solid three-phase interface instead. Currently, feasible strategies for the cost-effective, chemical-free, facile fabrication of flexible superoleophobic mesh enabling in-air oil–water separation are still rare.

In this article, we report the facile fabrication of kraft paper mesh for producing superoleophobic origami toward efficient oil–water separation. Natural hydrophilic kraft paper that features a porous structure, relative high elasticity, and tear resistance has been employed to fabricate such superoleophobic meshes. Taking advantage of the porous network, the kraft paper mesh can retain a large amount of water (2.5 times its weight under dry conditions). Thus, the kraft mesh is superoleophobic in water, and the water-infused kraft mesh can form a slippery surface that repels oil in air, which directly

enables the fishing out of oil droplets in water. Wet kraft mesh origami with both underwater superoleophobicity and in-air slippery wettability of oil droplets holds great promise for practical applications in oil–water separation.

■ EXPERIMENTAL METHODS

Fabrication of Kraft Paper Mesh by Direct Laser Drilling.

The programmable laser drilling of kraft mesh was carried out using a carbon dioxide laser engraving machine (JW6090, JG., China) with a laser power of 2.8 W (laser fluences of $\sim 350 \text{ W mm}^{-2}$). The laser scanning speed is 10 mm s^{-1} , and the scanning step length is 0.03 mm.

Characterization. The wettability of the kraft mesh was measured by using a Contact Angle System OCA 20 (DataPhysics Instruments GmbH, Germany) at ambient temperature. The underwater contact angles (CAs) of various oils and organic reagents were measured with a $4 \mu\text{L}$ droplet. Scanning electron microscope (SEM) images were obtained by using a field emission scanning electron microscope (JSM-7500F, JEOL, Japan). Confocal laser scanning microscope (CLSM) images were captured using a LEXT 3D measuring laser microscope (OLS4100, Olympus, Japan). Atomic force microscopy (AFM) images were obtained using a NanoWizard II BioAFM instrument (JPK Instruments AG, Berlin, Germany) in tapping mode.

Oil–Water Separation. The oil–water separation experiments have been carried out in different ways. First, we realized oil–water separation using a homemade device. A kraft mesh was sandwiched by two plastic tubes (syringe), and a bean oil–water mixture was poured into the upper tube. The separation was driven by gravity. Second, we made a dustpan-shaped origami using a kraft mesh. An oil droplet (corn oil) of $\sim 4 \mu\text{L}$ labeled by dyes was fished out of the water and transferred between two containers. For the third manner, a net-shaped origami was fabricated using the kraft mesh. A mixture of water and bean oil was poured out directly into the wet kraft mesh net for oil–water separation.

■ RESULTS AND DISCUSSION

Considering the porosity, high elasticity, and tear resistance, kraft paper has been chosen as a hydrophilic membrane for producing underwater superoleophobic meshes by direct laser drilling of microhole arrays. A CO_2 laser with a central wavelength of $10.6 \mu\text{m}$ was employed in the processing. Figure 1 shows a photograph of the kraft paper mesh (left image, 3 cm in diameter), a schematic illustration of the laser drilling process, and their applications in oil–water separation. The resultant kraft mesh demonstrates in-air hydrophilicity and

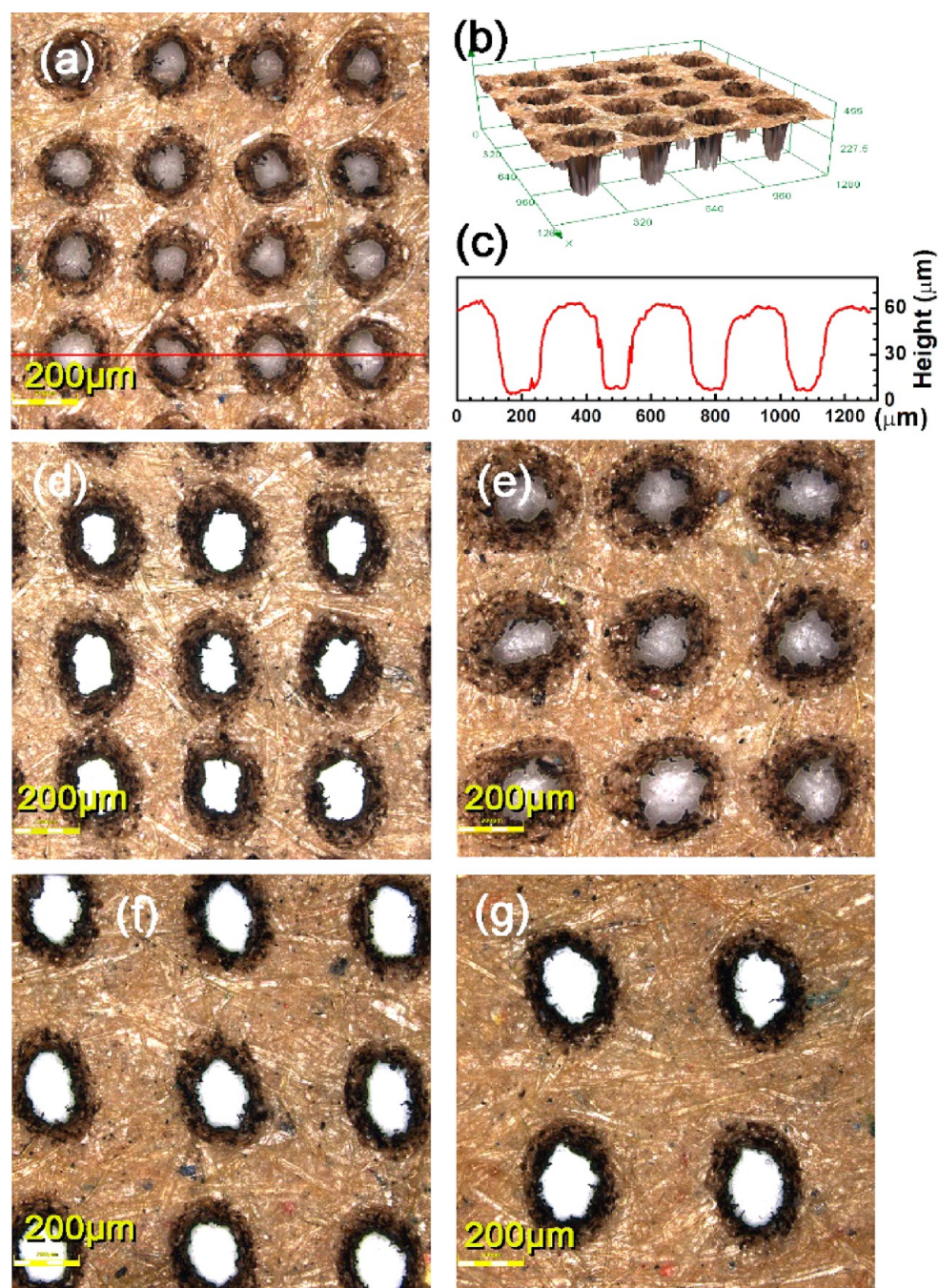


Figure 2. CLSM images of the kraft mesh with different hole sizes and distributions. (a) Tetragonal distribution of the microhole arrays with a $100\ \mu\text{m}$ hole diameter and a $200\ \mu\text{m}$ hole distance. (b) 3D image of the kraft mesh. (c) Profile of the kraft mesh along the red line in (a). (d–g) CLSM images of the kraft mesh with (d) a $125\ \mu\text{m}$ hole diameter and a $250\ \mu\text{m}$ hole distance, (e) a $150\ \mu\text{m}$ hole diameter and a $300\ \mu\text{m}$ hole distance, (f) a $175\ \mu\text{m}$ hole diameter and a $350\ \mu\text{m}$ hole distance, and (g) a $200\ \mu\text{m}$ hole diameter and a $400\ \mu\text{m}$ hole distance, respectively.

underwater superoleophobicity, and the water-infused wet kraft mesh behaves as a slippery surface for oil droplets. Additionally, the kraft mesh is highly flexible and can be made into various types of origami, which enables efficient oil–water separation through different means.

Direct laser drilling using a CO_2 laser enables the production of a large-area kraft mesh (A4 size, Figure S1) in a chemical-free, mask-free, cost-effective manner. Additionally, programmable laser drilling permits flexible tuning of the hole size and the distributions. In this work, we fixed the distribution of the microholes at tetragonal arrays and tuned the hole size and hole distance (distance between two hole boundaries) within a

certain range. Figure 2 shows the CLSM images of the kraft meshes with different hole sizes and distances. Here, we kept the ratio of hole size to hole distance at 1:2 and varied the hole size from 100 to $200\ \mu\text{m}$. 3D CLSM image of the kraft mesh confirms the presence of open holes (Figure 2b). The hole size and distance match the designed model well, as shown in the profile along the red line (Figure 2c). To choose an optimized mesh parameter to achieve better superoleophobicity, we further increase the hole size to 125 , 150 , 175 , and $200\ \mu\text{m}$, respectively (Figure 2d–g). The formation of the hole can be attributed to the laser ablation effect, and the minimum hole size (the resolution) is $\sim 75\ \mu\text{m}$ for the CO_2 laser. Further

decreases in the hole size can be achieved by using other laser sources, for instance, a femtosecond laser pulse. However, it would significantly increase the cost of the fabrication. Considering the cost, the efficiency, and the mechanical strength of the resultant kraft mesh, it is not necessary to pursue a smaller hole size because the kraft mesh might become fragile when the hole size is below $75\ \mu\text{m}$. (Mechanical strength is discussed in Figure 4c.)

To gain further insight into the surface morphology, we also characterized these kraft meshes using a scanning electron microscope (SEM, Figure 3). The kraft paper surface is quite

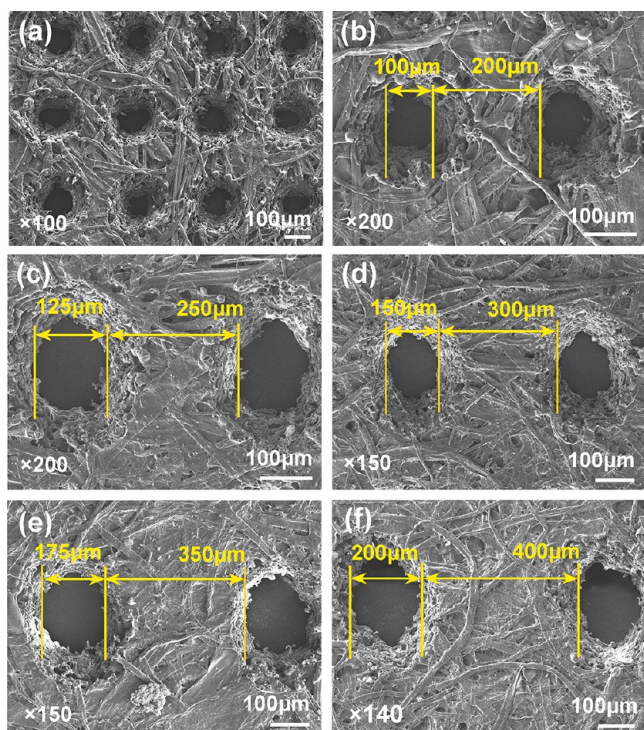


Figure 3. SEM images of the kraft mesh with different hole sizes and distances. (a, b) $100\ \mu\text{m}$ hole diameter and $200\ \mu\text{m}$ hole distance, (c) $125\ \mu\text{m}$ hole diameter and $250\ \mu\text{m}$ hole distance, (d) $150\ \mu\text{m}$ hole diameter and $300\ \mu\text{m}$ hole distance, (e) $175\ \mu\text{m}$ hole diameter and $350\ \mu\text{m}$ hole distance, and (f) $200\ \mu\text{m}$ hole diameter and $400\ \mu\text{m}$ hole distance.

rough. According to the AFM results, the roughness is $\sim 800\ \text{nm}$ (Figure S2). It consists of crossed microfibers (Figure S3a). After laser drilling, microholes formed as a result of the laser ablation effect. The formation of the microhole array further increase the surface roughness. The magnified SEM image shows that the hole is an inverted circular table shape. We measured the size and distance of the holes on the kraft mesh, which match the designed model well and are in good agreement with the CLSM images. However, we also note that some of the microfibers have been cut off due to the laser drilling treatments. This may destroy the microfiber network of the kraft papers and affect their mechanical strength. The section-view SEM image shows that the thickness of the kraft paper used in this work is $\sim 60\ \mu\text{m}$ (Figure S3b). To achieve higher elasticity and better tear resistance, thicker kraft paper can be employed for laser drilling.

The kraft paper is hydrophilic in air. A water droplet contact angle (CA) on the kraft paper surface is measured to be 74° (Figure S4). After laser drilling, the water CA further decreased

due to the increased surface roughness and the capillarity of the microholes. The kraft mesh with a $100\ \mu\text{m}$ hole size and a $200\ \mu\text{m}$ hole distance has a CA of 39° , indicating the in-air hydrophilicity. Notably, the water droplet CA on the kraft mesh is not unchanged. The water droplet can be gradually absorbed by the kraft mesh due to the porous microfiber networks.

To evaluate the superoleophobicity of the kraft meshes, we measured the underwater oil CAs on different surfaces. As shown in Figure 4a, the underwater oil CA on pristine kraft paper is 129° . After laser drilling, the underwater oil CAs increased obviously. They are all larger than 150° , reaching the underwater superoleophobic range. The increase in the oil CA can be mainly attributed to the presence of a microhole array. In addition, since the laser processing was performed under

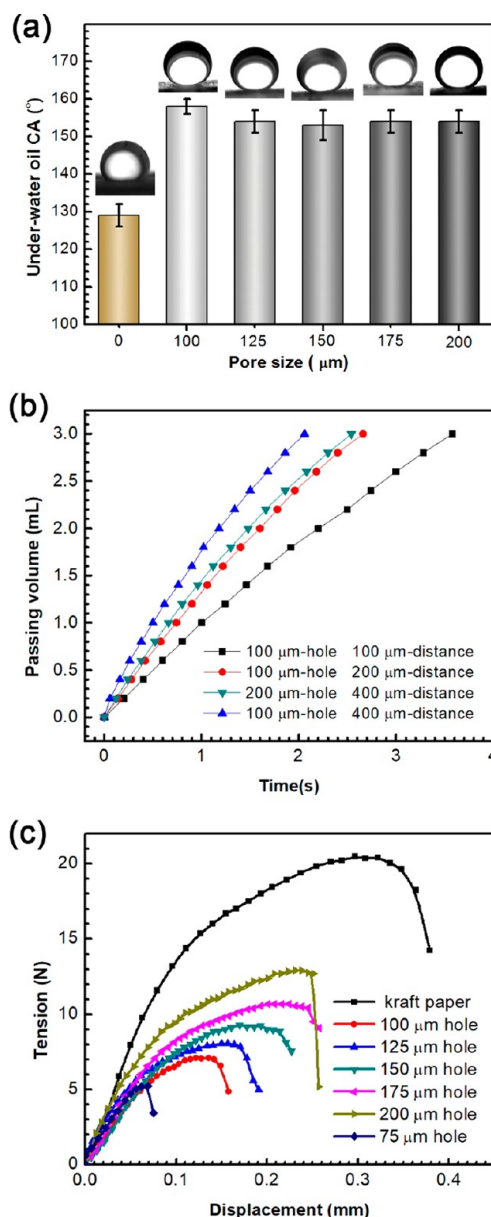


Figure 4. (a) Underwater oil (chloroform) CA on pristine kraft paper and kraft meshes with different hole sizes and distributions. (b) Water flow rate tests for kraft meshes with different hole sizes. (c) Tensile tests of pristine kraft paper and a kraft mesh with different hole sizes.

ambient conditions, the laser-ablation-induced oxidation may produce more oxygen groups, further increasing the hydrophilicity. As shown in the SEM images, laser drilling can increase the surface roughness. Additionally, when the kraft mesh was immersed in water, its surface could be considered to be a composite surface of kraft paper and water since water would fill in the holes and help to repel oil. The area portion of holes was calculated to be the same value of 8.72%. (For calculation details, see Figure S5.) Among these samples, the kraft mesh with a hole size of 100 μm has the highest underwater oil CA of $\sim 158^\circ$. Further increases in hole size and distance show unobvious effects on the surface wettability. These kraft meshes are all underwater superoleophobic.

Since the kraft mesh would be used for oil–water separation, the flow rate of water passing across the mesh is a very important parameter that affects the separation efficiency. Thus, we tested the water flow rate using four kraft meshes with different hole sizes and distances. Figure 4b shows the dependence of the water volume that passes across the meshes with time. Notably, the mesh with a 100 μm hole size/200 μm hole distance and the one with a 200 μm hole size/400 μm hole distance have similar flow rates since they have the same area portion of holes. To make a comparison, we also fabricated two additional kraft meshes with a 100 μm hole size/100 μm hole distance and a 100 μm hole size/400 μm hole distance, respectively. When we increase the portion of holes, the mesh with the 100 μm hole size/100 μm hole distance (area portion of holes, 19.6%; Figure S5) has a much higher flow rate, whereas the mesh with the 100 μm hole size/400 μm hole distance that has a much smaller hole portion (3.14%) has a much lower flow rate. Here, we have to point out that it is not necessary to pursue a high flow rate since a higher hole portion would result in relatively poor mechanical strength. Tensile tests show that pristine kraft paper possesses very good strength. When we stretch a kraft ribbon (60 μm in thickness and 1 cm in width) tight, the maximum tension is measured to be ~ 20 N (Figure 4c). After laser drilling, the mechanical strength of the kraft mesh decreased obviously since the drilling of microhole arrays has broken the microfibrer network of the kraft paper significantly. In this test, we keep the hole area portion at a constant value and vary the hole size from 75 to 200 μm . The mechanical strength decreased when the hole size (hole distance) increased because most of the microfibrers had been cut into small pieces when the hole distance decreased to a small value. The maximum tension for the kraft mesh with a 75 μm hole size/150 μm hole distance (Figure S6) is only one-fourth that of pristine kraft paper. Considering the underwater superoleophobicity, the water permeability, and the mechanical strength, we chose the kraft mesh with a 100 μm hole size/200 μm hole distance for the following experiments. Nevertheless, the other kraft meshes that feature different hole sizes, water permeability, and mechanical strength might find applications in different cases.

In addition to chloroform, we also measured the underwater CAs of different oil droplets using the kraft mesh with a 100 μm hole size/200 μm hole distance. Notably, most of the oils are lighter than water, thus we measured the CAs beneath the kraft mesh. As shown in Figure 5, the mesh shows underwater superoleophobicity for various oil droplets, and the CAs are generally in the range of 158 to 163 $^\circ$.

In addition to the large underwater oil CAs ($>150^\circ$), the kraft mesh also has a dynamic underwater oil-repelling property in sliding tests. As shown in Figure 6a–c, the sliding

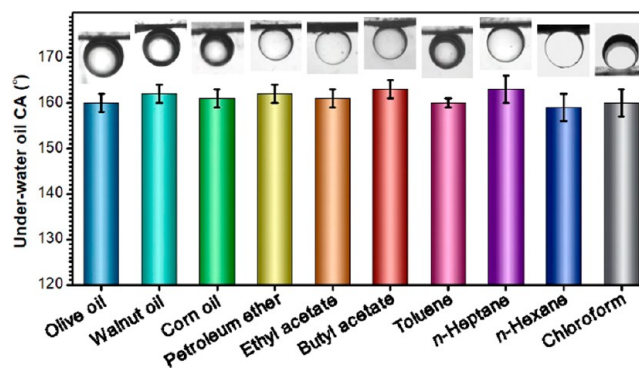


Figure 5. Underwater CAs of different oils based on the kraft mesh (100 μm hole size/200 μm hole distance). The insets are photographs of different oil droplets at the kraft mesh surface.

angle of a chloroform droplet based on the kraft mesh (100 μm hole size/200 μm hole distance) was measured to be 3 $^\circ$. The chloroform droplet can slide away rapidly from the kraft mesh. The underwater superoleophobicity and dynamic oil repelling property make it possible to use this kraft mesh in water–phase oil–water separation. However, the separation manner is limited to the underwater condition since the superoleophobicity is based on an oil/water/solid three-phase interface. Interestingly, when the kraft mesh is infused with water, it is also workable for oil–water separation in air. In this case, the oil wettability becomes complex. It changes to an air/oil/water/solid four-phase interface. We observed the slippery property of oil droplets on the solid–water heterogeneous surface of the wet kraft mesh. In air, the water-infused kraft mesh can form a slippery surface, and an oil droplet can slip away easily on a tilted surface (Figure 6d–f).

To gain deep insight into the wetting mechanism, we also investigated the different wetting models theoretically. When a water or oil droplet is in contact with the paper surface, the wettability can be explained by Wenzel's wetting model whereby the contact angle can be calculated according to the following equation

$$\cos \theta^* = \frac{r(\gamma_{SV} - \gamma_{SL})}{\gamma_{LV}} = r \cos \theta \quad (1)$$

where θ^* is the CA (water or oil droplet) on the rough kraft paper; r is the roughness factor (the ratio of the actual surface area to the projected area); γ_{SV} , γ_{SL} , and γ_{LV} are surface free energy of solid–vapor, solid–liquid, and liquid–vapor interfaces, respectively; and θ is the CA (water or oil droplet) on the theoretically flat kraft surface. According to our experimental results, the CAs of both a water droplet and an oil droplet measured in air are very small. As observed from the SEM images, the kraft paper consists of twining long fibers, forming a porous structure. Thus, a liquid droplet can easily wet the surface due to capillarity (Figure 7a). However, when the kraft paper is immersed in water first, water can wet the surface and even penetrate the microfibrer network. In this solid–water–oil three-phase system, the wettability of an oil droplet can be described as the underwater Cassie wetting state whereby the oil droplet is assumed to sit on a heterogeneous interface with water trapped within the microfibrer networks of the kraft paper (Figure 7b). In this case, the underwater CA of an oil droplet, $\theta^{*'}$, can be calculated from the following equation

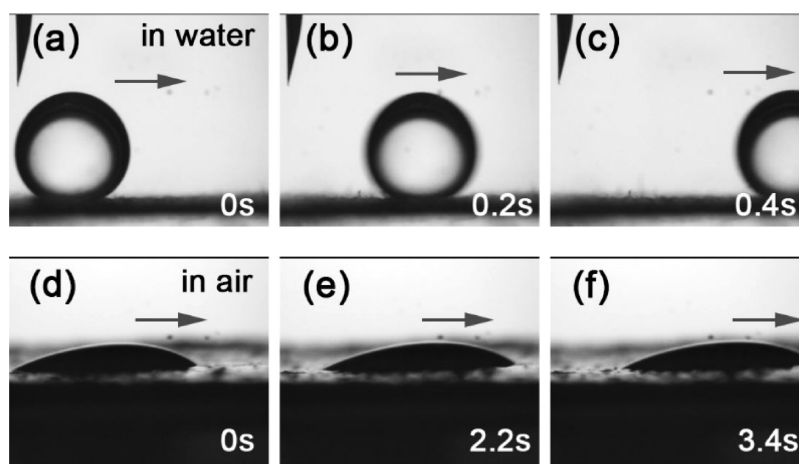


Figure 6. (a–c) Underwater sliding of an oil droplet on the kraft mesh at 0, 0.2, and 0.4 s, respectively. The sliding angle is 3°. (d–f) In-air slipping of an oil droplet on a wet kraft mesh surface at 0, 2.2, and 3.4 s, respectively. Tilted angle: 10°

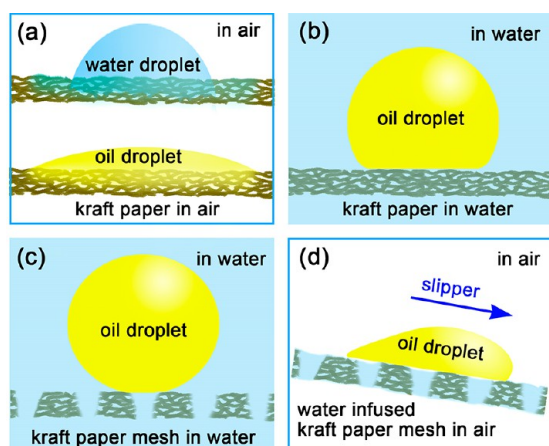


Figure 7. Schematic illustration of different wetting models of an oil droplet on kraft paper and kraft mesh. (a) Oil droplet and water droplet on kraft paper in air. (b) Oil droplet on kraft paper in water. (c) Oil droplet on kraft mesh in water. (d) Oil droplet on a water-infused kraft mesh in air.

$$\cos \theta^{*'} = f \cos \theta' + f - 1 \quad (2)$$

where f is the area fraction at the kraft paper and the oil droplet interface and θ' is defined as the underwater CA of a small oil droplet on the theoretically flat kraft surface. Note that θ' is a fixed value, and the decrease in the area fraction, f , can lead to an obvious increase in $\theta^{*'}$. In our work, we reduced the oil–kraft paper contacted area fraction by drilling holes. When the kraft paper mesh is immersed in water, these holes can be filled with water to form a heterogeneous interface with a much larger portion of water (Figure 7c). As a result, a much larger oil CA in the water medium can be achieved. Interestingly, when the kraft paper mesh is taken out of the water, it is still infused with water due to the capillarity. In this way, a slippery surface for oils formed naturally. According to our experimental results, the kraft paper mesh can retain 250% water when it is taken out of water. It is worth pointing out that the water-infused kraft paper mesh is quite important for oil–water separation. The as-formed oil slippery surface enables direct fishing out of oil droplets on the water surface and the mass-loss-free transfer of the oils elsewhere.

Taking advantage of unique superoleophobicity, the kraft meshes enable efficient oil–water separation in different ways.

First, we demonstrated the gravity-induced oil–water separation using a homemade setup. As shown in Figure 8, a mixture



Figure 8. Gravity-induced oil–water separation based on the kraft mesh. The kraft mesh with a 100 μm hole size/200 μm hole distance was sandwiched between two plastic tubes.

of bean oil and water was used for the separation. When we took off the stopper, water could be discharged. Water can pass through the hydrophilic kraft mesh easily. On the contrary, oil cannot pass through it due to the superoleophobicity. In this way, efficient oil–water separation has been realized (Supporting Information, Video S1). The oil content in the separated water is measured to be 0.05%. For gravity-induced oil–water separation, oil pressure resistance is an important parameter that can affect its practical use. In this work, the maximum oil pressure resistance of the superoleophobic kraft mesh is ~ 0.5 kPa (Figure S7). It further depends on the pore size of the kraft mesh.³⁸ As compared with membranes, underwater superoleophobic meshes have a much larger pore size, and thus the maximum oil pressure resistance is not too high. Nevertheless, owing to the larger pore size, the meshes feature high efficiency (a short separation time). To assess the separation capability of other oil–water mixtures, a kerosene–water mixture was also separated successfully using this kraft mesh (Figure S8).

Because of the porous structures, the kraft mesh can adsorb a large amount of water (2.5 times its weight under dry conditions). Thus, the kraft mesh infused with water becomes a slippery surface for oil droplets when it is placed in air. The unique dewetting property for oils enables the direct fishing out of oil droplets on the water's surface. Interestingly, by

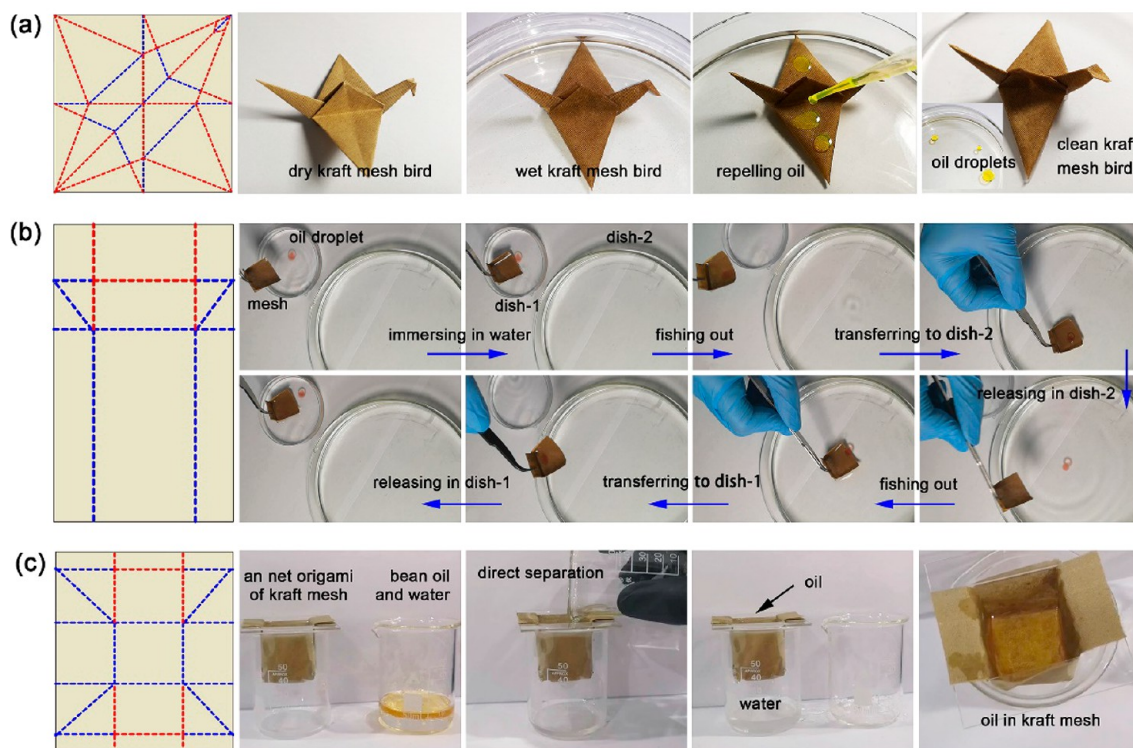


Figure 9. (a) Schematic illustration of the model for the folded Randlett's flapping bird origami. The photographs of the kraft mesh bird origami show that the wet origami repels oil in water. (b) Model for the folded dustpan-shaped origami and a series of photographs that show the fishing out of the oil droplet on water using the dustpan-shaped origami. (c) Model for the folded net origami and photographs that show the separation of the bean oil and water mixture using the kraft mesh net origami.

taking advantage of the flexibility, toughness, and good mechanical strength, we can make various origamis using kraft mesh for oil–water separation in air. With the help of the origami structures, oil/water separation can be achieved in a more convenient manner without the use of any glass/plastic instruments. In this experiments, we demonstrated three typical kraft mesh origamis. Figure 9a shows the schematic illustration of the model for fabricating a folded Randlett's flapping bird origami. The red and blue dashed lines indicate the mountain folds and the valley folds, respectively. Notably, the kraft mesh is robust enough to make complex origamis such as Randlett's flapping bird. When we wet the kraft mesh bird using water, it became origami with a slippery surface for oil droplets. We dropped several dye-labeled corn oil droplets, which can slip away easily, leaving a clean surface. To realize oil–water separation, we made a dustpan-shaped origami using a kraft mesh according to the model shown in Figure 9b. An oil droplet (corn oil) of $\sim 4 \mu\text{L}$ labeled by dyes can be directly fished out of the water and transferred between two containers freely. For the third manner, we fabricated a net-shaped origami using the kraft mesh (Figure 9c). A mixture of water and bean oil was poured out directly into the wet kraft mesh net for oil–water separation. All of the oil was collected within the kraft mesh net, and clear water was separated from the mixture. We further evaluated the water-retaining capability of our kraft mesh. Generally, it needs ~ 20 min to evaporate the water (Figure S9). The slippery kraft surface that is fully infused with water can work for at least 10 min in air. The swelling effect of the wet kraft mesh is not obvious, and the hole size remains almost unchanged after drying. Besides, the kraft mesh is robust after folding–unfolding 100 times, and the underwater oil CA remains almost unchanged (Figure S10).

CONCLUSIONS

Underwater superoleophobic kraft meshes have been successfully fabricated by direct laser drilling on kraft papers. Taking advantage of the flexibility of laser processing, both the hole size and hole distance can be tuned within a certain range. To optimize a suitable hole size and distribution for efficient oil–water separation, we tuned the hole size from 75 to 200 μm . We found that all of the kraft meshes show underwater superoleophobicity with underwater oil droplet CAs larger than 150° for a series of typical oils. We also evaluated the flow rate of water passing through the mesh and the mechanical strength of different meshes, both of which can be tuned by varying the hole sizes and area portion of the holes. Interestingly, the kraft meshes can adsorb a large amount of water and become a slippery surface for oil droplets, thus they enable efficient oil–water separation in different ways. Taking advantage of the flexibility, toughness, and good mechanical strength, we fabricated kraft mesh origamis and demonstrated oil–water separation using these origamis. Kraft mesh origami may find broad application in developing oil-repelling devices.

ASSOCIATED CONTENT

Supporting Information

The Supporting Information is available free of charge on the ACS Publications website at DOI: 10.1021/acs.langmuir.8b03541.

Photograph of large-area kraft paper mesh, AFM images of kraft paper, SEM and section-view SEM image of pristine kraft paper, wettability of kraft mesh and kraft paper, CLSM image/SEM image of a kraft paper mesh (75 μm hole size, 150 μm hole distance), oil pressure

resistance of the kraft mesh, and separation of a kerosene–water mixture (PDF)

AUTHOR INFORMATION

Corresponding Author

*E-mail: yonglaizhang@jlu.edu.cn.

ORCID

Yong-Lai Zhang: 0000-0002-4282-250X

Notes

The authors declare no competing financial interest.

ACKNOWLEDGMENTS

The authors acknowledge the National Key Research and Development Program of China and National Natural Science Foundation of China under grants 2017YFB1104300, 61775078, 61590930, and 61605055 for support. We also acknowledge the Natural Science Foundation of Jilin Province under grants 20180101061JC.

REFERENCES

- (1) Ariga, K.; Kawakami, K.; Ebara, M.; Kotsuchibashi, Y.; Ji, Q.; Hill, J. P. *New J. Chem.* **2014**, *38*, 5149–5163.
- (2) Wang, H.; Feng, Z.; Xu, B. *Chem. Soc. Rev.* **2017**, *46*, 2421–2436.
- (3) Oaki, Y. *Bull. Chem. Soc. Jpn.* **2017**, *90*, 776–788.
- (4) Kim, S.; Laschi, C.; Trimmer, B. *Trends Biotechnol.* **2013**, *31*, 23–30.
- (5) Liu, K.; Yao, X.; Jiang, L. Recent Developments in Bio-inspired Special Wettability. *Chem. Soc. Rev.* **2010**, *39*, 3240–3255.
- (6) Liu, K.; Jiang, L. Bio-inspired Design of Multiscale Structures for Function Integration. *Nano Today* **2011**, *6*, 155–175.
- (7) Lin, Y.; Han, J.; Cai, M.; Liu, W.; Luo, X.; Zhang, H.; Zhong, M. Durable and Robust Transparent Superhydrophobic Glass Surfaces Fabricated by a Femtosecond Laser with Exceptional Water Repellency and Thermostability. *J. Mater. Chem. A* **2018**, *6*, 9049–9056.
- (8) Liu, K.; Cao, M.; Fujishima, A.; Jiang, L. Bio-inspired Titanium Dioxide Materials with Special Wettability and Their Applications. *Chem. Rev.* **2014**, *114*, 10044–10094.
- (9) Li, J.; Zhou, X.; Li, J.; Che, L.; Yao, J.; Mchale, G.; Chaudhury, M. K.; Wang, Z. Topological Liquid Diode. *Sci. Adv.* **2017**, *3*, eaao3530.
- (10) Wang, J. N.; Liu, Y. Q.; Zhang, Y. L.; Feng, J.; Wang, H.; Yu, Y. H.; Sun, H. B. Wearable Superhydrophobic Elastomer Skin with Switchable Wettability. *Adv. Funct. Mater.* **2018**, *28*, 1800625.
- (11) Wang, J. N.; Liu, Y. Q.; Zhang, Y. L.; Feng, J.; Sun, H. B. Pneumatic Smart Surfaces with Rapidly Switchable Dominant and Latent Superhydrophobicity. *NPG Asia Mater.* **2018**, *10*, e470.
- (12) Jiang, H. B.; Zhang, Y. L.; Liu, Y.; Fu, X. Y.; Li, Y. F.; Liu, Y. Q.; Li, C. H.; Sun, H. B. Bioinspired Few-layer Graphene Prepared by Chemical Vapor Deposition on Femtosecond Laser-structured Cu Foil. *Laser Photon. Rev.* **2016**, *10*, 441.
- (13) Yong, J.; Chen, F.; Yang, Q.; Huo, J.; Hou, X. Superoleophobic Surfaces. *Chem. Soc. Rev.* **2017**, *46*, 4168–4217.
- (14) Zhao, Y.; Wu, Y.; Wang, L.; Zhang, M.; Chen, X.; Liu, M.; Fan, J.; Liu, J.; Zhou, F.; Wang, Z. Bio-inspired Reversible Underwater Adhesive. *Nat. Commun.* **2017**, *8*, 2218.
- (15) Zhao, Y.; Zhang, M.; Wang, Z. Underwater Superoleophobic Membrane with Enhanced Oil-water Separation, Antimicrobial, and Antifouling Activities. *Adv. Mater. Interfaces* **2016**, *3*, 1500664.
- (16) You, J.; Heo, J. S.; Lee, J.; Kim, H. S.; Kim, H. O.; Kim, E. A. Fluorescent Polymer for Patterning of Mesenchymal Stem Cells. *Macromolecules* **2009**, *42*, 3326–3332.
- (17) Xue, Z.; Cao, Y.; Liu, N.; Feng, L.; Jiang, L. Special Wettability Materials for Oil/Water Separation. *J. Mater. Chem. A* **2014**, *2*, 2445–2460.
- (18) Liu, Y.; Zhan, B.; Zhang, K.; Kaya, C.; Stegmaier, T.; Han, Z.; Ren, L. On-demand Oil/Water Separation of 3D Fe Foam by Controllable Wettability. *Chem. Eng. J.* **2018**, *331*, 278–289.
- (19) Liu, K.; Jiang, L. Metallic surfaces with special wettability. *Nanoscale* **2011**, *3*, 825–838.
- (20) Khosravi, M.; Azizian, S. Fabrication of an Oil Spill Collector Package by Using Polyurethane Foam Wrapped with Superhydrophobic ZnO Microrods/Carbon Cloth. *ChemPlusChem* **2018**, *83*, 455–462.
- (21) Liu, Y. Q.; Zhang, Y. L.; Fu, X. Y.; Sun, H. B. Bioinspired Underwater Superoleophobic Membrane Based on a Graphene Oxide Coated Wire Mesh for Efficient Oil/Water Separation. *ACS Appl. Mater. Interfaces* **2015**, *7*, 20930–20936.
- (22) Liu, Y. Q.; Han, D. D.; Jiao, Z. Z.; Liu, Y.; Jiang, H. B.; Wu, X. H.; Ding, H.; Zhang, Y. L.; Sun, H. B. Laser-Structured Janus Wire Mesh for Efficient Oil–water Separation. *Nanoscale* **2017**, *9*, 17933–17938.
- (23) Yong, J.; Chen, F.; Li, M.; Yang, Q.; Fang, Y.; Hou, J.; Hou, X. Remarkably Simple Achievement of Superhydrophobicity, Superhydrophilicity, Underwater Superoleophobicity, Underwater Superoleophilicity, Underwater Superaerophobicity, and Underwater Superaerophilicity on Femtosecond Laser Ablated PDMS Surfaces. *J. Mater. Chem. A* **2017**, *5*, 25249.
- (24) Liu, M.; Wang, S.; Wei, Z.; Song, Y.; Jiang, L. Bioinspired Design of a Superoleophobic and Low Adhesive Water/Solid Interface. *Adv. Mater.* **2009**, *21*, 665–669.
- (25) Xue, Z.; Wang, S.; Lin, L.; Chen, L.; Liu, M.; Feng, L.; Jiang, L. A Novel Superhydrophilic and Underwater Superoleophobic Hydrogel-coated Mesh for Oil/Water Separation. *Adv. Mater.* **2011**, *23*, 4270–4273.
- (26) Lian, Z.; Xu, J.; Wang, Z.; Yu, Z.; Weng, Z.; Yu, H. Nanosecond Laser-induced Underwater Superoleophobic and Underoil Superhydrophobic Mesh for Oil/Water Separation. *Langmuir* **2018**, *34*, 2981–2988.
- (27) Wu, W.; Huang, R.; Qi, W.; Su, R.; He, Z. Bioinspired Peptide-coated Superhydrophilic Poly(Vinylidene Fluoride) Membrane for Oil/Water Emulsion Separation. *Langmuir* **2018**, *34*, 6621–6627.
- (28) Yong, J.; Hou, J.; Chen, F.; Yang, Q.; Hou, X. Oil/water separation based on natural materials with super-wettability: recent advances. *Phys. Chem. Chem. Phys.* **2018**, *20*, 25140–25163.
- (29) Yong, J.; Chen, F.; Yang, Q.; Bian, H.; Du, G.; Shan, C.; Huo, J.; Fang, Y.; Hou, X. Oil-Water Separation: A Gift from the Desert. *Adv. Mater. Interfaces* **2016**, *3*, 1500650.
- (30) Yong, J.; Chen, F.; Huo, J.; Fang, Y.; Yang, Q.; Bian, H.; Li, W.; Wei, Y.; Dai, Y.; Hou, X. *ACS Omega* **2018**, *3*, 1395–1402.
- (31) Zhang, J.; Chen, F.; Yang, Q.; Yong, J.; Huo, J.; Fang, Y.; Hou, X. A Widely Applicable Method to Fabricate Underwater Superoleophobic Surfaces with Low Oil-adhesion on Different Metals by a Femtosecond Laser. *Appl. Phys. A: Mater. Sci. Process.* **2017**, *123*, 594.
- (32) Su, C.; Yang, H.; Song, S.; Lu, B.; Chen, R. A Magnetic Superhydrophilic/Oleophobic Sponge for Continuous Oil-water Separation. *Chem. Eng. J.* **2017**, *309*, 366–373.
- (33) Zhang, W.; Zhu, Y.; Liu, X.; Wang, D.; Li, J.; Jiang, L.; Jin, J. Salt-induced Fabrication of Superhydrophilic and Underwater Superoleophobic PAA-g-PVDF Membranes for Effective Separation of Oil-in-Water Emulsions. *Angew. Chem., Int. Ed.* **2014**, *53*, 856–860.
- (34) Yong, J.; Chen, F.; Yang, Q.; Jiang, Z.; Hou, X. A Review of Femtosecond-Laser-induced Underwater Superoleophobic Surfaces. *Adv. Mater. Interfaces* **2018**, *5*, 1701370.
- (35) Yin, K.; Chu, D.; Dong, X.; Wang, C.; Duan, J. A.; He, J. Femtosecond Laser Induced Robust Periodic Nanoripple Structured Mesh for Highly Efficient Oil-water Separation. *Nanoscale* **2017**, *9*, 14229–14235.
- (36) Ariga, K.; Li, J.; Fei, J.; Ji, Q.; Hill, J. P. Nanoarchitectonics for Dynamic Functional Materials from Atomic-/Molecular-Level Manipulation to Macroscopic Action. *Adv. Mater.* **2016**, *28*, 1251–1286.
- (37) Ariga, K.; Yamauchi, Y.; Rydzek, G.; Ji, Q.; Yonamine, Y.; Wu, K. C.-W.; Hill, J. P. Layer-by-layer Nanoarchitectonics: Invention, Innovation, and Evolution. *Chem. Lett.* **2014**, *43*, 36–68.

(38) Xue, Z. X.; Wang, S. T.; Lin, L.; Chen, L.; Liu, M. J.; Feng, L.; Jiang, L. A Novel Superhydrophilic and Underwater Superoleophobic Hydrogel-Coated Mesh for Oil/Water Separation. *Adv. Mater.* **2011**, *23*, 4270–4273.